BROOKHAVEN NATIONAL LABORATORY

December 1993 BNL- 49883

SW 9416

Scalar and Vector Meson Production in (K^-, K^+) Reactions on Nuclei

Carlo Gobbi[1,2], Carl B. Dover[1,3] and Avraham Gal[1,4]

[1]National Institute for Nuclear Theory, University of Washington
Seattle, WA 98195
[2]Center for Theoretical Physics, Sloane Physics Lab., Yale University
New Haven, CT 06511
[3]Physics Department, Brookhaven National Laboratory
Upton, New York 11973
[4]Racah Institute of Physics, The Hebrew University
Jerusalem 91904, Israel

ABSTRACT

An analysis of the observed double-strangeness-exchange (K^-, K^+) inclusive cross sections at 1.65 GeV/c on nuclear targets is presented. The K^+ momentum spectrum displays a low momentum peak centered around 600 MeV/c, which we interpret as due to the first order $K^-p \to \phi\Lambda$, $a_0\Lambda$ and $f_0\Lambda$ processes, followed by $\phi, a_0, f_0 \to K^+K^-$ decays. This hypothesis is shown to be consistent with the shape of the K^+ spectrum, its integrated cross section, and the A^α dependence observed for the (K^-, K^+) cross section on targets of mass number A. We predict a rapid energy dependence for the nuclear (K^-, K^+) process in the momentum region 1.4–1.8 GeV/c near the two-body thresholds for producing scalar (a_0, f_0) and vector (ϕ) mesons in K^-p collisions.

Submitted to *Physical Review C*

1. Introduction and Motivation

The advent of medium energy (1–2 GeV/c) kaon (K^-) beams at KEK in Japan and the Brookhaven AGS [1] has made possible the study of double strangeness exchange (K^-, K^+) reactions on nuclear targets. The initial thrust of the (K^-, K^+) experiments has been directed towards searches for the six quark H dibaryon [2-4] and $\Lambda\Lambda$ hypernuclei [5,6]. More recently, small angle (K^-, K^+) cross sections at $p_{K^-} = 1.65$ GeV/c were measured [7] on targets from C to Pb. These measurements yielded a rather surprising result: in addition to the quasi–free peaks in the K^+ momentum spectrum due to the elementary processes $K^-p \rightarrow K^+\Xi^-$, and $K^-p \rightarrow K^+\Xi^{*-}(1535)$, a very substantial peak at a low momentum $p_{K^+} \approx 600$ MeV/c was identified, with an integrated cross section in excess of that seen in the Ξ^- quasi–free region at higher momentum. The (K^-, K^+) cross section residing in the low momentum peak is far greater than that anticipated on the basis of second order strong processes, for instance $K^-p \rightarrow \pi^0\Lambda$ followed by $\pi^0 p \rightarrow K^+\Lambda$, as seen by explicit calculation or by analogy to the observed size of second order processes in the (K^-, π^+) reaction [8]. In this paper, we evaluate quantitatively the K^+ momentum spectrum which arises from the production/decay sequences

$$K^-p \rightarrow M\Lambda \tag{1a}$$

$$M \rightarrow K^+K^- \tag{1b}$$

taking place on a proton embedded in a nuclear target. Here the meson M is a scalar [$f_0(975)$ with quantum numbers $J^{\pi C}(I^G) = 0^{++}(0^+)$ or $a_0(980)$ with $0^{++}(1^-)$] or a vector [$\phi(1020)$ with $1^{--}(0^-)$]. The processes (1a,b) are depicted schematically in Fig. 1 for the ϕ. Since the production process (1a) is first order, and the branching ratio for the decay (1b) is substantial ($\sim 50\%$ for the ϕ), the (K^-, K^+) cross section arising from (1a,b) is intrinsically much larger than that characteristic of second order reactions, provided that (1a) is energetically possible. For instance, the free space two–body threshold for ϕ production in (1a) is $p_{K^-} = 1.76$ GeV/c, and hence the nuclear Fermi motion must be invoked in order to obtain a finite (K^-, K^+) nuclear cross section at the "sub–threshold" K^- momentum of 1.65 GeV/c. [7] This implies a rapid dependence of f_0, a_0 and ϕ production on p_{K^-} in the region near threshold. This predicted strong momentum dependence of the (K^-, K^+) cross section on nuclei serves as a decisive signature of the production

mechanism proposed here, as yet untested. The calculations reported here incorporate the effects of Fermi motion, the rapid energy dependence of the $K^-p \to M\Lambda$ cross sections near threshold, and initial and final state absorption of the K^- and the meson M, respectively. They quantify the rough estimates made in [8]. We also estimate the (smaller) effects of other first order processes such as $K^-p \to \phi\Sigma^0$, $K^*\Xi$. The sequence (1a,b) is found to provide a quantitative explanation of the basic features of the (K^-, K^+) spectrum:

i) the large observed magnitude of the cross section in the low momentum region ($p_{K^+} \simeq 600$ MeV/c)

ii) the shape of the K^+ spectrum (peak position and width)

iii) the observed A dependence of the (K^-, K^+) cross sections (approximately A^α, with $\alpha \approx 0.56 \pm 0.02$).

This paper is organized as follows: In Section 2, we provide a brief resumé of the experimental data on the $K^-p \to \phi\Lambda$ process, and develop a parametrization of the energy and angular dependence of the differential cross section. We make some simple estimates of the $K^-p \to f_0\Lambda$, $a_0\Lambda$ cross sections, for which no data are available. We then describe the procedure used to obtain the Fermi-averaged cross section used as input for the (K^-, K^+) calculations on nuclei. In Section 3, we present our estimates of the effective proton number $Z_{\rm eff}$ for the $K^-p \to \phi\Lambda$ reaction on nuclei. We obtain an approximate A^α dependence for $Z_{\rm eff}$, and investigate how α depends on the ϕ–nucleon cross section $\sigma_{\phi N}$. This enables us to understand the empirical value of α for (K^-, K^+) reactions on nuclei in terms of the (small) observed cross sections $\sigma_{\phi N}$ and σ_{K^+N}. Our estimates for the (K^-, K^+) double differential cross sections $d^2\sigma/d\Omega_L dp_{K^+}$ on C, Al, Cu, Ag and Pb nuclei are presented in Section 4, and compared with the data of Iijima *et al.* [7]. We also include some qualitative estimates of cross sections for second order processes in Section 5, and argue that perhaps these could be seen for K^- momenta below 1.4 GeV/c, where they are no longer masked by scalar and vector meson production. In Section 6, we summarize our results and present some suggestions for future experiments.

2. The Elementary $K^-p \to M\Lambda$ Processes and their Fermi Averages

A K^- meson in the momentum regime 1–2 GeV/c can initiate a variety of strong interaction processes. The thresholds for reactions leading to a K^+ in the final state are given in Table 1. The Ξ^- and $\Xi^{*-}(1530)$ production channels are both open at 1.65 GeV/c, and are reflected as quasifree peaks in the measured [7] (K^-, K^+) cross sections on nuclei. The three–body $K^+K^-\Lambda$ channel opens up at a slightly higher momentum, but will be activated with a nuclear target due to the Fermi motion of the protons. Considering K^+K^- pairs of different relative orbital angular momentum ℓ, we obtain various quasi–two–body reactions

$$K^- + p \to \begin{cases} \{f_0(975),\, a_0(980)\} & + \Lambda \to (K^+K^-)_{\ell=0} + \Lambda \\ \phi(1020) & + \Lambda \to (K^+K^-)_{\ell=1} + \Lambda \\ \{f_2'(1525),\, a_2(1320)\} & + \Lambda \to (K^+K^-)_{\ell=2} + \Lambda \end{cases} \tag{2}$$

For the energies considered here, only the scalar $S = \{f_0, a_0\}$ and vector $\{\phi\}$ mesons need be considered. From the decay branching ratios

$$BR(\phi \to K^+K^-) = 0.49, \quad BR(f_0 \to K^+K^-) = 0.11 \tag{3}$$

we see that ϕ production is likely to be the most prominent source of K^+ mesons in the (K^-, K^+) reaction, assuming that the $K^-p \to \phi\Lambda$ and $K^-p \to S\Lambda$ cross sections are comparable. There is no available data on f_0 and a_0 production with K^- beams for momenta of the order of 2 GeV/c, but one can make a rough estimate of the f_0/ϕ and a_0/ϕ cross section ratios as follows. We first determine the intrinsic coupling strengths $g_{K^+K^-f_0}$ and $g_{K^+K^-\phi}$ from the observed partial decay widths $\Gamma(f_0 \to K^+K^-) \approx 5.2$ MeV and $\Gamma(\phi \to K^+K^-) \simeq 2.2$ MeV by removing the phase space factors $(\mathrm{PS})_{\phi,\mathrm{f_0}}$:

$$g^2_{K^+K^-\phi} \equiv \Gamma(\phi \to K^+K^-)/(\mathrm{PS})_\phi, \quad \mathrm{g^2_{K^+K^-f_0}} \equiv \Gamma(\mathrm{f_0} \to \mathrm{K^+K^-})/(\mathrm{PS})_{\mathrm{f_0}} \tag{4}$$

We assume $(\mathrm{PS})_{\mathrm{f_0}} = \langle \mathrm{q} \rangle_{\mathrm{f_0}}$ and $(\mathrm{PS})_\phi = \mathrm{q}_\phi \mathrm{p_1}$, where $p_1 = x^2/(1+x^2)$ is a Blatt–Weisskopf penetrability for $\ell = 1$, $x = q_\phi R$, $R = 1$ fm, appropriate to the s and p–wave decay character of the f_0 and ϕ, respectively. We have $q_\phi = 127$ MeV/c and we obtain $\langle q \rangle_S$ by averaging over a Breit–Wigner shape for the f_0, using a non–relativistic approximation, for which no integration cutoff is necessary. This procedure yields

$$\langle q \rangle_S = \left(\frac{m_K}{\Delta^2 + \Gamma^2/4}\right)^{1/2} \left(\frac{\Gamma}{2} \mathrm{Re}\sqrt{\Delta + \frac{i\Gamma}{2}} - \Delta\, \mathrm{Im}\sqrt{\Delta + \frac{i\Gamma}{2}}\right) \tag{5}$$

where $\Delta = 2m_K - m_S$, and (m_S, Γ) are the mass and width of f_0 or a_0. We find

$$\langle q \rangle_S = \begin{cases} 58 \text{ MeV/c} & \text{for } f_0 \to K^+K^- \\ 77 \text{ MeV/c} & \text{for } a_0 \to K^+K^- \end{cases} \tag{6}$$

The ratios of coupling constants are then

$$g^2_{K^+K^-S}/g^2_{K^+K^-\phi} = \begin{cases} 1.51 & \text{for } f_0 \\ 1.38 \quad \frac{BR(a_0 \to K^+K^-)}{BR(f_0 \to K^+K^-)} & \text{for } a_0 \end{cases} \tag{7}$$

A crude estimate for the ratio $R_{S/\phi}$ of K^+'s arising via $\{f_0, a_0\}$ and ϕ production in the (K^-, K^+) reaction on nuclei is then

$$R_{S/\phi} = \frac{g^2_{K^+K^-S}}{g^2_{K^+K^-\phi}} \frac{BR(S \to K^+K^-)}{BR(\phi \to K^+K^-)} \tag{8}$$

Using Eq. (7), we obtain

$$R_{S/\phi} = \begin{cases} 0.34 & \text{for } f_0 \\ 0.31 \left[\frac{BR(a_0 \to K^+K^-)}{BR(f_0 \to K^+K^-)}\right]^2 & \text{for } a_0 \end{cases} \tag{9}$$

The value of $BR(a_0 \to K^+K^-)$ is not given by the Particle Data Group [9]; for the calculations reported here, we have simply assumed that $BR(a_0 \to K^+K^-) = BR(f_0 \to K^+K^-)$. This estimate indicates that f_0 and a_0 production could be a significant source of K^+ mesons, comparable in magnitude to the ϕ. This qualitative result is borne out by the more detailed calculations reported later.

From the values of $\langle q \rangle_S$, we compute effective masses m^*_S for the scalars, now considered as zero width particles:

$$m^*_S = 2\left(m^2_K + \langle q \rangle^2_S\right)^{1/2} = \begin{cases} 994.2 \text{ MeV} & \text{for } f_0 \\ 999.4 \text{ MeV} & \text{for } a_0 \end{cases} \tag{10}$$

These values of m^*_S correspond to effective K^- threshold momenta of {1.703, 1.715} GeV/c for $\{f_0, a_0\}$ production in the $K^-p \to S\Lambda$ reactions. The $\{f_0, a_0\}$ thresholds are a bit lower than that for ϕ production, which enhances somewhat the importance of scalar production for $p_{K^-} = 1.65$ GeV/c. In our subsequent cross section computations, we include scalar meson production, using the sharp effective masses m^*_S and the corresponding thresholds.

We now focus on the $K^-p \to \phi\Lambda$ reaction. Cross sections for this process have been measured at 2.24 GeV/c by London *et al.* [10], in the 2.1–2.7 GeV/c region by Lindsey

and Smith [11] and at higher momenta by Ayres *et al.* [12], Hoogland *et al.* [13], Haque *et al.* [14] and Aguilar-Benitez *et al.* [15]. The available information on total cross sections in the region below 2.8 GeV/c is displayed in Fig. 2, while the $K^-p \to \phi\Lambda$ angular distribution at 2.24 GeV/c [10] is shown in Fig. 3. The cross section is observed to be strongly peaked in the forward direction (i.e., the ϕ is produced at small angles with respect to the K^- beam direction). This is consistent with a dominant t–channel meson exchange (K^+, K^{*+}) mechanism. The backward peak which usually accompanies u–channel baryon exchange is absent in this case, because the coupling constant $g_{\phi NN}$ is small. In contrast, the reaction $K^-p \to \omega\Lambda$ displays a healthy backward peak, since $g_{\omega NN}$ is large. The lowest momentum for which $K^-p \to \phi\Lambda$ angular distributions have been measured is $p_{K^-} = 2.24$ GeV/c. From Fig. 3, we read off a c.m. forward cross section of about 30 μb/sr. In the lab system, the $K^-p \to \phi\Lambda$ angular distribution is much more strongly peaked at 0° than in the c.m. system, as we see from the relation

$$(d\sigma/d\Omega)_{L,0^\circ} \,/\, (d\sigma/d\Omega)_{\mathrm{cm},0^\circ} = \left(p_{\phi L}/p_{\phi,\mathrm{cm}}\right)^2 \tag{11}$$

For $p_{K^-} = 2.24$ GeV/c, we have $p_{\phi L} = 1.724$ GeV/c, $p_{\phi,\mathrm{cm}} = 0.465$ GeV/c, so that

$$(d\sigma/d\Omega)_{L,0^\circ} \,/\, (d\sigma/d\Omega)_{\mathrm{cm},0^\circ} \simeq 13.7, \tag{12}$$

leading to a lab forward cross section

$$(d\sigma/d\Omega)_{L,0^\circ} \simeq\ 410\mu\mathrm{b/sr} \tag{13}$$

for $K^-p \to \phi\Lambda$ at 2.24 GeV/c. This is a rather substantial cross section. As we approach threshold, the ϕ's become increasingly focused in a forward cone (in the lab frame) with maximum production angle $\theta^{\phi}_{L,\mathrm{max}}$. For a general two–body reaction $(\vec{k}_{L1}, m_1) + (0, m_2) \to (\vec{k}_{L3}, m_3) + (\vec{k}_{L4}, m_4)$, we have

$$\cos^2\theta_{L,\mathrm{max}} = \left[m_3^2\left(k_{L1}^2 + m_4^2\right) - \rho_1^2\right] / m_3^2 k_{L1}^2 \tag{14}$$

with $\rho_1 = E_{L1}m_2 + (m_1^2 + m_2^2 - m_3^2 - m_4^2)/2$, $E_{L1} = (m_1^2 + k_{L1}^2)^{1/2}$. The dependence of $\theta^{\phi}_{L,\mathrm{max}}$ on p_{K^-} is shown in Table 2. For instance, for $p_{K^-} \leq 1.9$ GeV/c, the ϕ's produced in the $K^-p \to \phi\Lambda$ reactions are narrowly focused in a forward cone with $\theta^{\phi}_{L,\mathrm{max}} \leq 16^\circ$. Since the lab momentum of the ϕ is rather substantial ($p_{\phi L} \geq 0.84$ GeV/c), even close to

threshold, the subsequent decay $\phi \to K^+K^-$ also produces K^+'s in a forward cone, with $\theta_L^{K^+} \leq \theta_{L,\mathrm{max}}^{K^+}$, measured with respect to the direction of the ϕ (see Fig. 1). We obtain $\theta_{L,\mathrm{max}}^{K^+}$ from Eq. (14) by setting $m_1 = m_\phi$, $m_2 = 0$, $m_3 = m_4 = m_K$. The values of $\theta_{L,\mathrm{max}}^{K^+}$ as a function of p_{K^-} are indicated in Table 2, both for ϕ production at 0° and at $\theta_{L,\mathrm{max}}^{\phi}$ (the latter in parentheses). Thus for $p_{K^-} \leq 1.9$ GeV/c, for instance, all K^+'s resulting from ϕ production and decay emerge at lab angles less than 35°, and most of these occupy the angular region 1.7°–13.6° measured by Iijima *et al.* [7].

Consider now a K^+ emerging at 0° from the decay $\phi \to K^+K^-$. Imposing energy conservation

$$E_{\phi L} = \left(m_K^2 + p_{K^+}^2\right)^{1/2} + \left(m_K^2 + \left(p_{\phi L} - p_{K^+}\right)^2\right)^{1/2}, \tag{15}$$

where $E_{\phi L} = (m_\phi^2 + p_{\phi L}^2)^{1/2}$, we find two solutions for the K^+ lab momentum p_{K^+}. We obtain

$$p_{K^+} = \begin{cases} 0.25,\ 0.59 \text{ GeV/c} & \text{at threshold} \\ 0.42,\ 0.82 \text{ GeV/c} & \text{for } p_{K^-} = 1.9 \text{ GeV/c} \\ 0.61,\ 1.11 \text{ GeV/c} & \text{for } p_{K^-} = 2.21 \text{ GeV/c} \end{cases} \tag{16}$$

The larger momenta correspond to a K^+ produced at 0° in the c.m. system, while the smaller values are for 180° c.m. production. The value $p_{K^-} = 2.21$ GeV/c, for a proton target at rest, corresponds to the same c.m. energy $s^{1/2} = 2.32$ GeV as for an encounter of a 1.65 GeV/c K^- with a proton moving opposite to the beam direction at the Fermi momentum $p_F = 270$ MeV/c. Thus Fermi motion at 1.65 GeV/c leads to an effective momentum interval $1.76 \leq p_{K^-} \leq 2.21$ GeV/c. In this regime, the decay K^+'s at 0° populate the region $0.25 \leq p_{K^+} \leq 1.1$ GeV/c, from Eq. (16), with a peak expected around $p_{K^+} \simeq 0.6$ GeV/c. This corresponds to the position of the "low momentum" bump seen by Iijima *et al.* [7] in the (K^-, K^+) reaction on nuclei, and lends qualitative support to our interpretation of this structure as due to meson production and decay. The width of this structure reflects Fermi broadening.

At higher momenta, the Σ and $K^*(892)$ production channels open up (see Table 1), and additional contributions to the K^+ spectrum are expected from ϕ and K^* decay, for which we have

$$BR\left(K^{*+} \to K^+\pi^0\right) \approx 1/3, \quad BR\left(K^{*0} \to K^+\pi^-\right) \approx 2/3 \tag{17}$$

At 2.1 GeV/c, Ayres *et al.* [12] give a total cross section ratio

$$\sigma\left(K^- p \to \phi\Sigma^0\right)/\sigma\left(K^- p \to \phi\Lambda\right) \approx 0.1 \tag{18}$$

Noting that Σ production can occur on neutrons as well as protons, and using the isospin relation

$$\sigma\left(K^- n \to \phi\Sigma^-\right) = 2\sigma\left(K^- p \to \phi\Sigma^0\right), \tag{19}$$

we estimate a ratio of approximately 0.3 for decays K^+'s arising from Σ/Λ production at 2.1 GeV/c. Thus as the K^- momentum rises above about 1.8–1.9 GeV/c, Σ production will start to become significant as a source of K^+'s.

The K^* production cross sections have been measured near threshold by London *et al.* [10], Dauber *et al.* [16] and DeBellefon *et al.* [17]. For example, at 2.1 GeV/c, Dauber *et al.* [16] give

$$\sigma\left(K^- p \to K^{*+}\Xi^-\right) \simeq \sigma\left(K^- p \to K^{*0}\Xi^0\right) \simeq 25\ \mu\text{b}, \tag{20}$$

whereas London *et al.* [10] obtained a K^{*0}/K^{*+} ratio of $\sim 1/2$ at 2.24 GeV/c, with $\sigma(K^{*+}) \simeq 34\ \mu$b. Thus at 2.1 GeV/c, we have

$$\sigma\left(K^- p \to K^{*+}\Xi^-\right)/\sigma\left(K^- p \to \phi\Lambda\right) \approx 1/3 \tag{21}$$

As for Σ's, the production of K^{*+}'s will start to become an important source of K^+'s above $p_{K^-} = 1.8 - 1.9$ GeV/c.

For our purposes, we require a smooth parametrization of the $K^- p \to \phi\Lambda$ cross section down to threshold. We represent the total cross section data shown in Fig. 2 as

$$\sigma_{K^- p \to \phi\Lambda} = B q\, e^{-\beta q} \tag{22}$$

where (B, β) are constants and q is the c.m. momentum of the ϕ in the final state. This form exhibits the correct behavior $\sigma \sim q$ near threshold and drops smoothly to zero at high q. The fit is performed by fitting an assumed value $q_{\max}$ at which the cross section peaks at a value $\sigma^{\max}_{K^- p \to \phi\Lambda}$. Because of the rather large error bars of the data, $q_{\max}$ is not well determined, so we assume a range of possibilities. The constants are then determined by

$$\beta = 1/q_{\max}, \quad B = e\,\sigma^{\max}_{K^- p \to \phi\Lambda}/q_{\max} \tag{23}$$

The resulting parameters (β, B) for Models 1, 2 and 3 are listed in Table 3, along with the lab momentum $p_{K^-}^{\max}$ corresponding to the peak cross section $\sigma_{K^-p\to\phi\Lambda}^{\max}$. The cross sections resulting from Models 1, 2 and 3 are shown in Fig. 2 as solid, dashed and short-dashed lines, respectively.

Now consider the c.m. angular distribution for the $K^-p \to \phi\Lambda$ reaction. We start with a standard parametrization

$$\left(\frac{d\sigma}{d\Omega}\right)_{\rm cm}^{K^-p\to\phi\Lambda} = A\, e^{\alpha(t-t_{\rm min})} = A\, e^{2pq\alpha(\cos\theta-1)} \tag{24}$$

where t is the four- momentum transfer, $t_{\rm min}$ is its value at $\theta_{\rm cm} = 0°$, and (p, q) are the c.m. momenta in the initial and final states, respectively. We approximate (24) by a simpler form

$$\left(\frac{d\sigma}{d\Omega}\right)_{\rm cm}^{K^-p\to\phi\Lambda} \approx A\, e^{\tilde{\alpha}(\cos\theta-1)} \tag{25}$$

where the energy dependence of the cross section is carried by A, and $\tilde{\alpha}$ is taken to be energy independent. We determine $\tilde{\alpha}$ from the data of London *et al.* [10] at 2.24 GeV/c as

$$\tilde{\alpha} = -\ln\left[\left(\frac{d\sigma}{d\Omega}\right)_{\rm cm}^{90°} \Big/ \left(\frac{d\sigma}{d\Omega}\right)_{\rm cm}^{0°}\right] \approx 1.8, \tag{26}$$

where we have estimated the 0° and 90° c.m. cross sections from Fig. 3 as 30 μb/sr and 5 μb/sr, respectively. In Eq. (25), the parameter A is obtained from the value of $\tilde{\alpha}$ and the total cross section σ via the relation

$$A = \frac{\tilde{\alpha}}{2\pi}\sigma\,(1-\exp(-2\tilde{\alpha}))^{-1} \approx \frac{\tilde{\alpha}\sigma}{2\pi} \simeq 0.3\sigma \tag{27}$$

The form (25) is shown as a solid line in Fig. 3, and is seen to provide an acceptable fit to the rather uncertain data of London *et al.* [10]. Transforming Eq. (25) to the lab frame, we display our predicted lab differential $K^-p \to \phi\Lambda$ cross section in Fig. 4, for lab momenta in the range $p_{K^-} = 1.8 - 2.2$ GeV/c. The lab cross sections are seen to evolve smoothly as a function of p_{K^-}.

For the $K^-p \to S\Lambda$ cross sections, no data are available, so we have to rely on some guesswork. We assume that scalar meson as well as ϕ production is dominated by K^+ exchange. This is essentially the peripheral model, which assumes the dominance of the t-channel exchange of longest range. We then expect a total cross section ratio

$$\sigma_{K^-p\to S\Lambda}/\sigma_{K^-p\to\phi\Lambda} \approx g^2_{K^+K^-S}/g^2_{K^+K^-\phi} \tag{28}$$

where the ratio of coupling constants is taken from Eq. (7). For the f_0 and a_0, we adopt the same parametrization of σ in terms of q and $\cos\theta$ as for the ϕ, assuming the same values for β and $\tilde{\alpha}$, and appropriately modifying A and B, which are proportional to σ. Experimental measurements of the $K^-p \to K^+K^-\Lambda$ cross sections are required in the threshold region, in order to isolate the $\{f_0, a_0\}$ and ϕ components, and test our simple hypothesis. There could be interesting interference effects between the 0^+ and 1^- mesons in the differential cross sections, which may shed some light on the structure of the f_0 and a_0. Such measurements should be pursued at the Brookhaven AGS, where the highest intensity K^- beams are available in the key momentum range of 1.7–2 GeV/c.

For the evaluation of the $K^-p \to \phi\Lambda, S\Lambda$ processes on a nuclear target, it is crucial to perform an average over the Fermi motion of the nucleons in the nucleus. Following Dalitz and Gal [18], we split the nucleon lab momentum $\vec{p}_N$ into a component p_z along the K^- beam axis and a transverse component $\vec{p}_T$ in the (x, y) plane. We can then write the square of the c.m. energy for a K^-p collision as

$$\begin{aligned} s &= (E_{K^-} + E_N)^2 - (\vec{p}_K + \vec{p}_N)^2 \\ &\simeq s_0 + \left(\frac{E_{K^-} + E_N(p_z)}{m_N} - 1\right) p_T^2 \simeq s_0 + \frac{4}{5} E_{K^-} \frac{p_F^2}{2m_N} \end{aligned} \tag{29}$$

where $s_0 = (E_{K^-} + E_N(p_z))^2 - (p_{K^-} + p_z)^2$ and $E_N(p_z) = (m_N^2 + p_z^2)^{1/2}$. Using the Fermi momentum $p_F = 270$ MeV/c and $p_{K^-} = 1.65$ GeV/c, we find that the fractional correction $(\frac{4}{5} E_{K^-} \frac{p_F^2}{2m_N})/s_0(p_z = 0) \simeq 0.0126$ to s, due to the transverse components of the nucleon Fermi motion, is very small. We neglect $\vec{p}_T$ in the following, and perform a Fermi average of the $K^-p \to \phi\Lambda$ and $S\Lambda$ lab differential cross sections over a distribution $\phi(p_z)$ of the z component of nucleon momentum. We assume the Fermi gas form

$$\phi(p_z) = \frac{3}{4p_F}\left(1 - p_z^2/p_F^2\right) \quad \text{for } -p_F \le p_z \le +p_F \tag{30}$$

The Fermi–averaged cross sections are then

$$\langle \frac{d\sigma}{d\Omega_L}(\theta) \rangle = \int_{-p_F}^{+p_F} dp_z \phi(p_z) \frac{d\sigma}{d\Omega_L}(s_0, \theta), \tag{31}$$

where we use the form (25), transformed to the lab frame, and a parametrization of the decay $\phi \to K^+K^-$ described in more detail in Section 5, to evaluate $d\sigma/d\Omega_L(s_0, \theta)$. To

compare with the results of Iijima *et al.*, we need to carry out a further averaging over the angular integral $\theta_1 \leq \theta \leq \theta_2$, with $\theta_1 = 1.7°$, $\theta_2 = 13.6°$. Thus we have

$$\langle \frac{d\sigma}{d\Omega_L} \rangle = \int_{\theta_1}^{\theta_2} d\theta \langle \frac{d\sigma}{d\Omega_L}(\theta) \rangle / (\theta_2 - \theta_1) \tag{32}$$

In fact, the average done is somewhat more sophisticated in that the actual θ grid has to be chosen such that, after accounting for the K^+ opening angle with respect to the ϕ direction, the overall K^+ angle with respect to the K^- beam direction is limited as above. This procedure is described in Section 4. The resulting Fermi and angle–averaged cross sections $\langle d\sigma/d\Omega_L \rangle_{1,2,3}$ for Models 1, 2 and 3 (see Table 3) are given in Table 4 as a function of p_{K^-}. One notes a rapid growth of $\langle d\sigma/d\Omega_L \rangle$ as p_{K^-} increases, and a leakage of cross section to the "sub–threshold" region $p_{K^-} \leq 1.76$ GeV/c, due to Fermi motion.

3. The Effective Proton Number $Z_{\rm eff}$

Let us first consider ϕ production. In the plane wave approximation, the (K^-, ϕ) nuclear cross section will be proportional to the number of target protons Z. Due to the fact that the K^- and ϕ can be absorbed in the nuclear medium, only an effective number of protons $Z_{\rm eff} < Z$ are operative. We estimate $Z_{\rm eff}$ in the Glauber approximation, for which

$$Z_{\rm eff} = \frac{Z}{A} \int d^3\vec{r} \rho(r) \exp \left[-\sigma_{K^-N} \int_{-\infty}^{z} \rho(x, y, z')\, dz' - \sigma_{\phi N} \int_{z}^{\infty} \rho(x, y, z')\, dz' \right] \tag{33}$$

where σ_{K^-N} and $\sigma_{\phi N}$ are averaged K^-N and ϕN total cross sections and $\rho(r)$ is the nuclear density normalized according to $\int d^3r \rho(r) = A$. We assume $\sigma_{K^-} \simeq 29$ mb, as in Iijima *et al.* [7]. The ϕ cross section is not well determined, but values $\sigma_{\phi N} = (8.3 \pm 0.5)$ mb and (8.8 ± 2.2) mb have been quoted by Behrend *et al.* [19] and Bailey *et al.* [20], from studies of photoproduction and the A dependence of inclusive ϕ production, respectively. For our considerations, we have considered a range of values $6 \leq \sigma_{\phi N} \leq 10$ mb. Equation (33) does not include the possibility that the decay $\phi \rightarrow K^+K^-$ may occur in the nucleus, and hence $\sigma_{\phi N}$ is replaced by σ_{K^+N} for part of the meson trajectory through the nucleus. However, in the low momentum region $p_{K^+} \simeq 0.6$ GeV/c of most relevance here, we have

$\sigma_{K^+N} \approx \sigma_{\phi N}$, and hence our results will change very little. Since the scalar mesons are much broader than the ϕ ($\Gamma_{f_0} = 47$ MeV, $\Gamma_{a_0} = 57$ MeV, $\Gamma_\phi = 4.4$ MeV), they have an increased probability of decaying in the nucleus, and again σ_{K^+N} enters in Eq. (33). In our calculations, we have simply made the assumption that $Z_{\rm eff}$ is the same for a_0, f_0 and ϕ production.

For the nuclear densities $\rho(r)$, we have assumed a three parameter Fermi form

$$\rho(r) = \rho_0 \left(1 + wr^2/R^2\right) \left(1 + \exp\left((r - R)/a\right)\right)^{-1} \tag{34}$$

The parameters (w, R, a), obtained from Refs. [21,22], are given in Table 5. We assume that the neutron and proton densities have the same radial shape. To test the sensitivity of $Z_{\rm eff}$ to the assumed shape of $\rho(r)$, we have also considered an harmonic oscillator density for ^{12}C:

$$\rho(r) = \rho_0 \left(1 + \alpha k^2 y^2\right) \exp\left(-k^2 y^2\right) \tag{35}$$

with $k = [3(2 + 5\alpha)/2(3 + 3\alpha)]^{1/2}$, $y = r/R$, $\alpha = 4/3$, $R = 2.47$ fm.

Our results for $Z_{\rm eff}$ are shown in Table 6. For ^{12}C, we see that the value of $Z_{\rm eff}$ for the two choices (34) and (35) for $\rho(r)$ are practically identical. The variations of $Z_{\rm eff}$ with $\sigma_{\phi N}$ are more significant, of order 10% for ^{12}C and 30% for ^{208}Pb. The A dependence of $Z_{\rm eff}$ may be approximated as

$$Z_{\rm eff} = C\, A^\alpha \tag{36}$$

A fit to the $Z_{\rm eff}$ values in Table 6 gives $\alpha \simeq 0.47$ for $\sigma_{\phi N} = 8.5$ mb, but the quality of the fit is not very good. As $\sigma_{\phi N}$ is decreased, α increases. In the limits of strong/weak cross sections, we expect

$$\alpha = \begin{cases} 1 & \text{for } \sigma_{K^-N} = \sigma_{\phi N} = 0 \\ 2/3 & \text{for large } \sigma_{K^-N}, \sigma_{\phi N} = 0 \\ 1/3 & \text{for large } \sigma_{K^-N}, \sigma_{\phi N} \end{cases} \tag{37}$$

We note that the (K^-, K^+) cross sections of Iijima *et al.* [7], which are proportional to $Z_{\rm eff}$, are described by an A dependence of the form (36), with $\alpha = 0.38 \pm 0.03$ for the upper peak in the K^+ spectrum and $\alpha = 0.56 \pm 0.02$ for the lower bump. Since the upper peak corresponds to $K^-p \to K^+\Xi^-$ quasi-free production, and the cross sections $\sigma_{K^-N} = 29$ mb, $\sigma_{K^+N} = 18.4$ mb [7] are both relatively large, one expects α close to 1/3, characteristic of a first order process with strong absorption Eq. (37). This is what

is observed. The fact that the lower momentum bump is characterized by an α closer to 2/3 was advanced by Iijima *et al.* [7] as an argument for the dominance of second order processes. As we see later, the magnitude of such processes falls far short of the data, so this suggestion is untenable. Alternatively, we can interpret the lower bump as the result of the first order $K^- p \to \phi\Lambda, f_0\Lambda, a_0\Lambda$ reactions, and the larger α as the signature of the small value of $\sigma_{\phi N}$, as in Eq. (37). For $\sigma_{\phi N} \simeq 4$ mb, we obtain $\alpha \simeq 0.56$, the value given by Iijima *et al.* [7] for the lower bump.

4. The (K^-, K^+) Cross Section on Nuclei

We have now assembled the ingredients for an evaluation of the (K^-, K^+) differential cross section and the K^+ momentum spectrum. The (K^-, K^+) double differential cross section assumes the form

$$\frac{d^2\sigma}{d\Omega_{K+} dp_{K+}} = Z_{\rm eff} \sum_M \left\langle \frac{d\sigma}{d\Omega_L} \right\rangle_{K^- p \to M\Lambda} BR\left(M \to K^+K^-\right) S_M\left(p_{K+}, \theta_{K+}\right) \qquad (38)$$

where $S_M(p_{K+}, \theta_{K+})$ is the shape function, normalized to unity when integrated over p_{K+}, characterizing the K^+ momentum spectrum arising from the production and decay of meson M. Note that we are discussing processes involving quasifree production of a Λ. Thus the additional kinematical factor α, which accompanies a formula analogous to Eq. (38) for Λ's in bound states [23], is absent here.

The cross sections have been evaluated by a Monte Carlo procedure, using a randomly selected nucleon momentum within a Fermi sphere, ϕ production angle, and K^+ decay angles. We first pick a value of p_z according to the weight function $\phi(p_z)$ of Eq. (30). We then compute an effective K^- lab momentum $\tilde{p}_{K^-}$ corresponding to a collision with a nucleon at rest:

$$\tilde{p}_{K^-} = \left(E_N\left(p_z\right) p_{K^-} - E_{K^-} p_z\right) / m_N \qquad (39)$$

where $E_N(p_z)$ is the same as in Eq. (29). If $\tilde{p}_{K^-} \geq 1.76$ GeV/c, the threshold for the $K^- p \to \phi\Lambda$ reaction (and similarly for f_0 and a_0), we continue the procedure and pick a random value of $\cos\theta$ for the ϕ in the c.m. system, using a weight function proportional

to the ϕ production cross section of Eq. (25). We transform θ to the lab frame using the relation

$$\tan\theta_L^\phi = p_{\phi,\mathrm{cm}} \sin\theta/\gamma \left(p_{\phi,\mathrm{cm}} \cos\theta + \beta E_{\phi,\mathrm{cm}}\right), \tag{40}$$

where $\beta = \tilde{p}_{K^-}/(\tilde{E}_{K^-} + m_N)$ and $\gamma = (1-\beta^2)^{-1/2}$.

We now consider the decay $\phi \to K^+K^-$, as shown in Fig. 1. The decay angular distribution for the ϕ, in its rest frame, will be of the form $\sum_m P(m)|Y_{1m}(\theta,\phi)|^2$, where $P(m)$ is the m–state probability distribution, subject to $\sum_m mP(m) = 0$. In the analogous ρ meson production process $\pi^- p \to \rho^0 n$, the ρ^0 is known to be created mostly in an $m = 0$ state, as a consequence of the dominance of long range pseudoscalar pion exchange in the t–channel [24]. For such a "peripheral" mechanism, the ρ may be viewed as an intermediate state in a reaction $\pi + \pi \to \rho \to \pi + \pi$. In this case, there is no z–component of angular momentum in the initial state and hence $m = 0$, leading to a ρ decay angular distribution proportional to $|Y_{10}(\theta,\phi)|^2$. In analogy to ρ production, we expect the $K^- p \to \phi\Lambda$ reaction to be driven mostly by pseudoscalar kaon exchange, and hence the $m = 0$ polarization state would also dominate for the ϕ. Hence, we assume that the ϕ decay amplitude varies as $Y_{10} \sim \cos\theta_{\mathrm{cm}}^{K^+}$. Note that vector meson exchange (ω in ρ^0, K^* in ϕ production) leads mostly to $m = \pm 1$ states [24]. For the scalar mesons f_0 and a_0, the decay amplitudes are isotropic in the meson rest frame, since the K^+K^- pair must be in a relative s–wave.

We thus choose a random value of $\cos\theta_{\mathrm{cm}}^{K^+}$ in the range $[-1,+1]$, with a weight proportional to $\cos^2\theta_{\mathrm{cm}}^{K^+}$ for the ϕ and 1 for the f_0 and a_0. We then transform to the lab frame where the ϕ has a momentum $p_{\phi L}$ and the K^+ is emitted with an angle $\theta_L^{K^+}$ with respect to a z–axis defined by the ϕ direction. We have

$$\tan\theta_L^{K^+} = p^r_{K^+} \sin\theta_{\mathrm{cm}}^{K^+}/\gamma_\phi \left(p^r_{K^+} \cos\theta_{\mathrm{cm}}^{K^+} + \beta_\phi E^r_{K^+}\right) \tag{41}$$

where $p^r_{K^+} = \frac{1}{2}(m_\phi^2 - 4m_K^2)^{1/2}$ is the K^+ momentum in the rest frame of the ϕ, $E^r_{K^+} = (m^2_{K^+} + p^r_{K^+})^{1/2}$, $\beta_\phi = p_{\phi L}/E_{\phi L}$, and $\gamma_\phi = (1-\beta_\phi^2)^{-1/2}$.

To test if the K^+ lies in the angular region measured by Iijima *et al.* [7],

$$1.7^\circ \le \theta\left(K^-, K^+\right) \le 13.6^\circ,$$

we note that

$$\cos\theta\left(K^-, K^+\right) = \cos\theta_L^\phi \cos\theta_L^{K^+} - \sin\theta_L^\phi \sin\theta_L^{K^+} \sin\phi_L^{K^+} \tag{42}$$

where $\phi_L^{K^+}$ is the azimuthal angle of the K^+. We pick a random value of $\phi_L^{K^+}$ in the interval $[0, 2\pi]$ and, using the angles $\theta_L^{K^+}$ and θ_L^{ϕ} chosen above, we check whether $\theta(K^-, K^+)$ is in the desired range. If it is, we compute the K^+ lab momentum p_{K^+} from the relation

$$p_{K^+} = p'_{K^+} \frac{\sin\theta_{\rm cm}^{K^+}}{\sin\theta_L^{K^+}} \tag{43}$$

and enter a count of weight $W = W_1 W_2 W_3$ in the appropriate 50 MeV/c bin of Iijima *et al.* [7]. The W_i are the weights associated with the random choices of p_z, $\cos\theta$ and $\{\cos\theta_{\rm cm}^{K^+}, \phi_L^{K^+}\}$, respectively.

Our Model 2 results for the (K^-, K^+) cross sections $d^2\sigma/d\Omega_L dp_{K^+}$ at 1.65 GeV/c on targets of ^{12}C, ^{27}Al, ^{63}Cu, ^{107}Ag and ^{208}Pb are shown in Fig. 5, together with the data of Iijima *et al.* [7]. The first order $K^-p \to M\Lambda$ processes are seen to deliver K^+'s at a rate even larger than that for the $K^-p \to K^+\Xi^-$, $K^+\Xi^{*-}(1530)$ reactions, but peaked at low momentum. The magnitude and shape of the K^+ spectrum is seen to be in reasonable agreement with the data, although the peak occurs at somewhat too small a momentum. We note that about 1/2 of the predicted (K^-, K^+) cross section is made up by the $K^-p \to f_0(975)\Lambda$, $a_0(980)\Lambda$ processes. We emphasize that this is only a rough guess, since no two–body data on f_0 and a_0 production exist. The separate contribution of the ϕ is shown in Fig. 6 as the lowest solid curve. The two hump structure of the ϕ curve reflects the fact that a K^+ from ϕ decay can have two distinct lab momenta, as shown in Eq. (16). When the scalars are added, the extended opening angle of the K^+ tends to wipe out such a distinction, and the two hump structure is largely washed out.

The model dependence of our predictions is shown in Fig. 6 for the (K^-, K^+) reaction on a ^{107}Ag target. The differences between Models 1, 2 and 3 (see Table 3) are only of order 20%. In Fig. 6, the Ξ^- and $\Xi^{*-}(1530)$ quasifree cross sections estimated by Iijima *et al.* [7] are subtracted from the data. The agreement with the data is reasonable. We expect that some of the discrepancy above $p_{K^+} = 700$ MeV/c would disappear if we included the $K^-p \to \phi\Sigma^0$ process (see Eqs. (18) and (19)), which tends to produce higher momentum K^+'s.

In Table 7, we display the angle–averaged differential cross sections $\langle d\sigma/d\Omega_{K^+}\rangle$ at 1.65 GeV/c for Models 1,2 and 3, obtained by integrating the solid curves in Fig. 5 over the momentum range $0.35 \le p_{K^+} \le 0.95$ GeV/c. The data [7] are shown as $\langle d\sigma/d\Omega_{K^+}\rangle_{\rm exp}$ in

the right-hand column. The contribution of Ξ^- and $\Xi^{*-}(1530)$ production in the same region of p_{K^+}, shown in parentheses, should be subtracted before the experimental and theoretical results are compared. The agreement is seen to be good. The growth of $\langle d\sigma/d\Omega_{K^+}\rangle$ with A follows that of $Z_{\rm eff} \sim A^\alpha$, as in Eq. (36). The results in Figs. 5,6 and Table 7 correspond to a choice of $\sigma_{\phi N} = 8.5$ mb, which yields $\alpha = 0.47$, not far from the experimental value $\alpha = 0.56 \pm 0.02$. This discrepancy is not serious, since we could obtain the observed α value by reducing $\sigma_{\phi N}$ somewhat, as remarked in Section 3.

The Fermi-averaged $K^-p \to \phi\Lambda$ cross section depends very strongly on p_{K^-}, as shown in Table 4. This will also be true for f_0 and a_0 production. The value of $\langle d\sigma/d\Omega_L\rangle$ becomes negligible (< 1 μb/sr) below 1.34 GeV/c, which serves as an effective threshold for the onset of ϕ production in nuclei. This rapid momentum dependence is reflected in the (K^-, K^+) cross sections on nuclei, which are predicted to be augmented by a factor of about 20 as p_{K^-} varies from 1.4 to 2 GeV/c. This striking increase is illustrated in Fig. 7 for the (K^-, K^+) reaction on ^{12}C and ^{208}Pb targets. For ^{12}C, these predictions could be compared with data recently taken at 1.4 and 1.8 GeV/c in an experiment at the Brookhaven AGS [25]. The strong dependence on p_{K^-} is a characteristic signature of the first order $K^-p \to \phi\Lambda, f_0\Lambda, a_0\Lambda$ processes and represents a key point in our interpretation of the (K^-, K^+) data.

5. Second Order Processes

Iijima *et al.* [7] have suggested that the low momentum peak in the K^+ spectrum may be due to second order processes. These are of the type

$$K^-N \to MY, \quad MN \to K^+Y' \tag{44}$$

where $M = \{\pi, \eta, \rho, \omega\}$ is a pseudoscalar or vector meson and $\{Y, Y'\} = \{\Lambda, \Sigma, \Sigma(1385), \Lambda(1405)\}$ is a hyperon or hyperon resonance. We now argue that this possibility does not offer a consistent interpretation of either the magnitude of the (K^-, K^+) cross section in the low momentum region or the shape of the K^+ spectrum.

For $p_{K^-} = 1.65$ GeV/c, the first stage reactions $K^-N \to MY$ of Eq. (44) are all energetically allowed except for $K^-N \to (\rho, \omega) + (\Lambda(1405), \Sigma(1385))$. For instance, the

$K^-p \to \pi^0\Lambda$, $\pi^0\Sigma^0$, $\eta\Lambda$ and $\omega\Lambda$ reactions at 1.65 GeV/c lead to meson lab momenta at $\theta = 0°$ of 1.53, 1.26, 1.42 and 1.25 GeV/c, respectively. If we also consider the second stage reaction $MN \to K^+Y'$ at 0°, we obtain the K^+ momenta shown in Table 8. We note that the value of p_{K^+} at 0° is essentially independent of M, for a given choice of Y and Y'. We further observe that the processes with the largest cross section, as obtained from the tabulation of Flaminio *et al.* [26], correspond to $M = \pi^0$, $\{Y, Y'\} = \{\Lambda, \Lambda\}$, $\{\Lambda, \Sigma^0\}$ or $\{\Sigma^0, \Lambda\}$. For these, the K^+ emerges with a *high momentum* $p_{K^+} \geq 0.93$ GeV/c, and these processes will be masked by the Fermi-broadened first order quasi-free $K^-p \to K^+\Xi^-$ reaction. As seen from Table 8, the only processes which would contribute to the K^+ peak around 500–700 MeV/c involve $\{Y, Y'\} = \{\Sigma, \Sigma\}$, $\{\Lambda, \Sigma(1385)\}$, or $\{\Lambda, \Lambda(1405)\}$. Some of the cross sections for the $K^-N \to \pi\Sigma$, $\pi N \to K^+\Sigma$ sequence on a single NN pair were estimated by Iijima *et al.* [7] from the formula [8,27]:

$$\left[\frac{d\sigma}{d\Omega_L}\right]^{0°}_{(K^-,K^+)} \approx \frac{2\pi\alpha_1\alpha_2\xi}{p_M^2}\left\langle\frac{1}{r^2}\right\rangle \left[\frac{d\sigma}{d\Omega_L}\right]^{0°}_{K^-N\to MY} \left[\frac{d\sigma}{d\Omega_L}\right]^{0°}_{MN\to K^+Y'} \tag{45}$$

where $\langle\frac{1}{r^2}\rangle$ is the inverse square radial separation of the NN pair, $\alpha_{1,2}$ are kinematical factors, and ξ arises from an integral over the angular distribution of the two processes. We have [7]

$$\left[\frac{d\sigma}{d\Omega_L}\right]^{0°}_{K^-+NN\to K^++\Sigma\Sigma} \approx \begin{cases} 0.12\ \mu\text{b}/sr & \text{for } K^-p \to \pi^+\Sigma^-, \pi^+p \to K^+\Sigma^+ \\ 0.02\ \mu\text{b}/sr & \text{for } K^-p \to \pi^-\Sigma^+, \pi^-p \to K^+\Sigma^- \\ 0.04\ \mu\text{b}/sr & \text{for } K^-p \to \pi^+\Sigma^-, \pi^+n \to K^+\Sigma^0 \end{cases} \tag{46}$$

An upper limit for the contribution of these processes to the (K^-, K^+) reaction on nuclei is obtained in plane wave approximation if we multiply by the number of pp or np pairs $Z(Z-1)$ or ZN, respectively:

$$\left[\frac{d\sigma}{d\Omega_L}\right]^{0°}_{^{12}\text{C}(K^-,K^+)} \approx 0.14Z\,(Z-1) + 0.04NZ \approx 5.6\mu\text{b}/sr \tag{47}$$

This is much smaller than the observed ^{12}C cross section [7] of 289 ± 12 μb/sr, integrated over the region $0.35 \leq p_{K^+} \leq 0.95$ GeV/c. Even if we sum over all $K^-N \to \pi Y$, $\pi N \to K^+Y$ processes ($Y = \Lambda, \Sigma$), as estimated in Ref. [7], we obtain only $0.3Z(Z-1)+0.2NZ \approx$ 16 μb/sr in place of Eq. (47), still more than an order of magnitude smaller than the observed cross section. Due to absorptive effects, we might expect a considerably smaller

second order cross section of order $0.3Z_{\rm eff}(Z_{\rm eff}-1)+0.2N_{\rm eff}Z_{\rm eff} \simeq 3.3$ μb/sr. Thus a rough estimate of the ratio of second to first order (K^-, K^+) reactions is

$$\frac{0.3Z_{\rm eff}\,(Z_{\rm eff}-1)+0.2N_{\rm eff}Z_{\rm eff}}{75Z_{\rm eff}} \simeq 1.5\times 10^{-2} \quad \text{for} \quad {}^{12}\text{C} \tag{48}$$

where 75 μb/sr represents the sum of $K^-p \to K^+\Xi^-$, $K^+\Xi^{*-}(1530)$ differential cross sections at 1.65 GeV/c.

A similar ratio has been seen in the (K^-, π^+) reaction on a ^{3}He target [8]. Here, the second order $pp(K^-, \pi^+)\Lambda\Lambda$ cross section at 20°, due to the $K^-p \to \pi^0\Lambda$, $\pi^0 p \to \pi^+ n$ sequence, is about 7 μb/sr [8]. The first order $K^-p \to \pi^+\Sigma^-$ cross section is about 1 mb/sr, yielding a ratio of order 7×10^{-3}.

Our qualitative conclusion is that second order (K^-, K^+) reactions occur on nuclei, but only at the level of 1% of the first order processes at 1.65 GeV/c. Since the strength of the low momentum bump in the (K^-, K^+) reaction is observed [7] to exceed that of the quasi-free $K^-p \to K^+\Xi^-$ peak, we conclude that it must arise from a first order rather than a second order reaction.

6. Conclusions

The measured forward angle (K^-, K^+) cross sections on nuclei at 1.65 GeV/c display a striking low momentum peak in the K^+ spectrum [7]. We interpret this peak as due primarily to first order $K^-p \to M\Lambda$ reactions, followed by the decay $M \to K^+K^-$. Here M is a scalar (f_0, a_0) or vector (ϕ) meson. We are able to explain the peak position and width of the K^+ spectrum with this mechanism, as well as the approximate magnitude and A dependence of the observed cross section. The production of the a_0 and f_0 mesons is estimated to contribute about one half of the K^+ peak at low momentum. We predict a rapid energy dependence of the low momentum component of the (K^-, K^+) cross section in the region $p_{K^-} = 1.4 - 2$ GeV/c, as we pass through the free space thresholds for the $K^-p \to M\Lambda$ reactions. Nuclear Fermi motion lowers the effective threshold for ϕ production to about 1.35–1.4 GeV/c. The rapid p_{K^-} dependence of the (K^-, K^+) cross section in the region of low K^+ momentum is a principal signature of the $K^-p \to M\Lambda$ mechanism. This merits an experimental test.

On the basis of the data in Ref. [7], Imai [5] reported that the number of single Λ hyperfragments observed in coincidence with events in the two K^+ peaks corresponds to a 1% sticking probability for the upper peak and about 4% for the lower peak. This preponderance of Λ hypernuclear formation in conjunction with low momentum K^+'s follows naturally from our $K^-p \rightarrow M\Lambda$ hypothesis, since the $M \rightarrow K^-K^+$ decay, if it occurs in the nucleus, produces K^-'s centered around 600 MeV/c, which can readily produce hypernuclei via the $K^-N \rightarrow \pi\Lambda$ process. The experimental search for the formation of $\Lambda\Lambda$ and Ξ hypernuclear states in (K^-, K^+) reactions on nuclei should be vigorously pursued.

Acknowledgments

This collaborative effort was initiated while the authors were attending Program 8, Strangeness in Hadronic Systems, at the National Institute for Nuclear Theory of the University of Washington in Seattle. We would like to thank Wick Haxton, Ernie Henley and Jerry Miller for their hospitality and support during our stay in Seattle. One of us (CG) was partially supported by a fellowship of the Fondazione Della Riccia, Italy. Another (AG) is partially supported by the Basic Research Foundation administered by the Israel Academy of Sciences. We would also like to acknowledge the help of Toru Iijima, who supplied us with numerical tables of the (K^-, K^+) cross sections.

References

1. P.H. Pile *et al.*, Nucl. Instr. and Methods in Phys. Research A321, 48 (1992).
2. S. Aoki *et al.*, Phys. Rev. Lett. 65, 1729 (1990).
3. P.D. Barnes, Nucl. Phys. A547, 3c (1992);
   A.T.M. Aerts and C.B. Dover, Phys. Rev. D29, 433 (1984).
4. R.L. Jaffe, Phys. Rev. Lett. 38, 195 (1977); 38, 617(E) (1977).
5. S. Aoki *et al.*, Prog. Theor. Phys. 85, 1287 (1991);
   K. Imai, Nucl. Phys. A547, 199c (1992).
6. C.B. Dover, D.J. Millener, A. Gal and D.H. Davis, Phys. Rev. C44, 1905 (1991);
   D. Zhu, C.B. Dover, A. Gal and M. May, Phys. Rev. Lett. 67, 2268 (1991).
7. T. Iijima *et al.*, Nucl. Phys. A546, 588 (1992).
8. R.E. Chrien, C.B. Dover and A. Gal, Czech. J. Phys. 42, 1089 (1992).
9. M. Aguilar–Benitez *et al.*, Phys. Rev. D45, No. 11, Part II (1992).
10. G.W. London *et al.*, Phys. Rev. 143, 1034 (1966).
11. J.S. Lindsey and G.A. Smith, Phys. Rev. 147, 913 (1966).
12. D.S. Ayres *et al.*, Phys. Rev. Lett. 32, 1463 (1974).
13. W. Hoogland *et al.*, Nucl. Phys. B21, 381 (1970).
14. M. Haque *et al.*, Phys. Rev. 152, 1148 (1966).
15. M. Aguilar–Benitez *et al.*, Phys. Rev. D6, 29 (1972).
16. P.M. Dauber, J.P. Berge, J.R. Hubbard, D.W. Merrill and R.A. Muller, Phys. Rev. 179, 1262 (1969).
17. A. DeBellefon *et al.*, Nuovo Cim. 28A, 289 (1975).
18. R.H. Dalitz and A. Gal, Phys. Lett. B64, 154 (1976).
19. H. Behrend *et al.*, Phys. Lett. B56, 408 (1975).
20. R. Bailey *et al.*, Z. Phys. C22, 125 (1984).
21. Landolt–Börnstein: Numerical Data and Functional Relationships in Science and Technology, New Series, Ed. K.-H. Hellwege, Group I, Vol. 2, Springer Verlag, Berlin (1967).

22. C.W. DeJager, H. DeVries and C. DeVries, Atomic Data and Nuclear Data Tables 14, 479 (1974).

23. E.H. Auerbach *et al.*, Ann. Phys. 148, 381 (1983).

24. S. Gasiorowicz, *Elementary Particle Physics*, Wiley and Sons, Inc., New York (1966); p. 317, Eq. (20.2).

25. R.E. Chrien, private communication.

26. V. Flaminio, I.F. Graf, J.D. Hansen, W.G. Moorhead and D.R.O. Morrison, Compilation of Cross-Sections, II. K^+ and K^- Induced Reactions, CERN-HERA Report 79-02, Geneva (1979).

27. C.B. Dover, Nukleonika 25, 521 (1980); note that the result for the second order cross section given in Eq. 14 of this paper should be divided by 4π.

Table Captions

Table 1: Thresholds for K^-–induced reactions on a proton target.

Table 2: Maximum lab angles $\theta^{\phi}_{L,\max}$, $\theta^{K^+}_{L,\max}$ and ϕ lab momentum $p_{\phi L}$ at $\theta^{\phi}_{L} = 0°$, as a function of K^- momentum p_{K^-}. The numbers in parentheses refer to a ϕ produced at an angle $\theta = \theta^{\phi}_{L,\max}$. Of the two solutions for $p_{\phi L}(0°)$, we list the one with largest momentum, with the corresponding value of $\theta^{K^+}_{L,\max}$.

Table 3: Parameters of Models 1, 2 and 3 for the $K^-p \to \phi\Lambda$ total cross section.

Table 4: Fermi–averaged lab differential cross sections for the $K^-p \to \phi\Lambda$ reaction as a function of K^- lab momentum for Models 1, 2 and 3. The cross sections are averaged over the angular interval $1.7° \leq \theta_L \leq 13.6°$, as measured by Iijima et al. [7] at 1.65 GeV/c, according to the discussion at the end of Section 2.

Table 5: Parameters of Fermi density distributions for various nuclei.

Table 6: Effective proton number $Z_{\rm eff}$ for the $K^-p \to \phi\Lambda$ reaction on nuclei for several values of the ϕN total cross section $\sigma_{\phi N}$. The values of $Z_{\rm eff}$ in parentheses refer to a harmonic oscillator density for ^{12}C; the other values correspond to the three parameter Fermi distributions of Table 5.

Table 7: Lab differential cross sections for the (K^-, K^+) reaction at 1.65 GeV/c on nuclear targets, based on the sequences $K^-p \to M\Lambda$, $M \to K^+K^-$, with $M = \{f_0, a_0, \phi\}$, compared with the data of Iijima et al. [7]. The theoretical cross sections are averaged over the angular interval $1.7° \leq \theta_{K^+} \leq 13.6°$, as in Iijima et al., and integrated over the K^+ momentum range $0.35 \leq p_{K^+} \leq 0.95$ GeV/c. The data are tabulated for the same K^+ angular and momentum range. Predictions for models 1,2 and 3 of the $K^-p \to \phi\Lambda$ reaction are shown. The numbers in parentheses next to $\langle d\sigma/d\Omega_{K^+}\rangle^{\rm exp}$ refer to the integrated Ξ^- and $\Xi^{*-}(1530)$ quasifree lab cross sections, in the same region of p_{K^+}, as calculated by Iijima et al.

Table 8: Momenta p_{K^+} arising from second order processes at 0°, for $p_{K^-} = 1.65$ GeV/c.

Table 1

Reaction	Threshold K^- momentum (lab)
$K^- + p \to K^+ + \Xi^-$	1.05 GeV/c
$K^- + p \to K^+ + \Xi^{*-}(1530)$	1.52
$K^- + p \to K^+ + K^- + \Lambda$	1.69
$K^- + p \to f_0 + \Lambda$	1.70
$K^- + p \to a_0 + \Lambda$	1.72
$K^- + p \to \phi + \Lambda$	1.76
$K^- + p \to \phi + \Sigma^0$	1.95
$K^- + p \to K^{*+}(892) + \Xi^-$	1.95

Table 2

p_{K^-} (GeV/c)	$p_{\phi L}(0°)$ (GeV/c)	$\theta^{\phi}_{L,\max}$	$\theta^{K^+}_{L,\max}$ (ϕ at 0°)
1.76	0.84 (0.84)	0°	18.3° (18.3°)
1.8	1.03 (0.835)	8.8°	14.8° (18.3°)
1.9	1.24 (0.825)	16.4°	12.2° (18.6°)
2.0	1.40 (0.81)	21.1°	10.8° (18.9°)
2.1	1.54 (0.80)	24.6°	9.8° (19.2°)

Table 3

Model	β (GeV/c)$^{-1}$	$B(\mu$b/GeV/c)	$p^{\max}_{K^-}$ (GeV/c)	$\sigma^{\max}_{K^-p\to\phi\Lambda}(\mu$b)
1	2.017	411.21	2.3	75
2	1.450	315.31	2.8	80
3	1.615	395.04	2.6	90

Table 4

p_{K^-} (GeV/c)	$\langle d\sigma/d\Omega_L\rangle_1$ (μb/sr)	$\langle d\sigma/d\Omega_L\rangle_2$	$\langle d\sigma/d\Omega_L\rangle_3$
1.3	0.00	0.00	0.00
1.32	0.19	0.15	0.19
1.34	2.92	2.34	2.90
1.4	17.08	14.10	17.28
1.5	57.25	48.22	58.76
1.6	90.96	78.65	95.13
1.65	118.58	102.73	124.17
1.7	126.89	111.75	134.43
1.8	161.51	144.05	172.62
1.9	186.33	169.15	201.63
2.0	206.10	190.06	225.49

Table 5

Nucleus	R (fm)	a (fm)	w
^{12}C	2.355	0.5224	-0.149
^{27}Al	3.07	0.52	0
^{63}Cu	4.20	0.55	0
^{107}Ag	5.12	0.52	0
^{208}Pb	6.40	0.54	0.32

Table 6

Nucleus	$Z_{\rm eff}(\sigma_{\phi N} = 6$ mb)	$Z_{\rm eff}(\sigma_{\phi N} = 8.5$ mb)	$Z_{\rm eff}(\sigma_{\phi N} = 10$ mb)
^{12}C	3.06 (3.10)	2.90 (2.94)	2.82 (2.85)
^{27}Al	5.24	4.86	4.66
^{63}Cu	8.44	7.59	7.15
^{107}Ag	10.41	9.10	8.44
^{208}Pb	13.47	11.05	10.41

Table 7

Nucleus	$\langle d\sigma/d\Omega_{K^+}\rangle_1$ (μb/sr)	$\langle d\sigma/d\Omega_{K^+}\rangle_2$	$\langle d\sigma/d\Omega_{K^+}\rangle_3$	$\langle d\sigma/d\Omega_{K^+}\rangle$ exp
^{12}C	242.7 (246.1)	210.3 (213.2)	254.2 (257.7)	289 $\pm$ 12 (65)
^{27}Al	406.8	352.4	425.9	472 $\pm$ 35 (107)
^{63}Cu	635.2	550.3	665.2	719 $\pm$ 50 (166)
^{107}Ag	761.6	659.8	797.5	1032 $\pm$ 53 (193)
^{208}Pb	954.1	826.6	999.1	1357 $\pm$ 99 (219)

Table 8

Processes	p_{K^+} (GeV/c)
$K^-p \to \pi^0\Lambda; \pi^0 p \to K^+\Lambda, K^+\Sigma^0$	1.238, 1.106
$K^-p \to \eta\Lambda; \eta p \to K^+\Lambda, K^+\Sigma^0$	1.234, 1.130
$K^-p \to \omega\Lambda; \omega p \to K^+\Lambda, K^+\Sigma^0$	1.225, 1.108
$K^-p \to \pi^0\Sigma^0; \pi^0 p \to K^+\Lambda, K^+\Sigma^0$	0.929, 0.773
$K^-p \to \pi^0\Lambda; \pi^0 p \to K^+\Sigma^0(1385), K^+\Lambda(1405)$	0.714, 0.656

Figure Captions

Fig. 1: A contribution to the (K^-, K^+) reaction on nuclear targets, via the production-decay sequence $K^-p \to \phi\Lambda$, $\phi \to K^+K^-$ initiated on a target proton in the nucleus.

Fig. 2: Total cross section for the $K^-p \to \phi\Lambda$ reaction as a function of K^- lab momentum p_{K^-}. The experimental data are taken from Lindsey and Smith [11]. The solid, dashed and short-dashed lines correspond to Models 1, 2 and 3, respectively, as defined by Eqs. (22) and (23) and Table 3.

Fig. 3: Differential cross section in the c.m. system as a function of $\cos\theta_{\rm c.m.}$ for the $K^-p \to \phi\Lambda$ reaction at 2.24 GeV/c. The data are taken from London et al. [10], and the theoretical curve corresponds to the parametrization of Eq. (25).

Fig. 4: Predicted lab differential cross section for the process $K^-p \to \phi\Lambda$ as a function of the ϕ lab angle θ_L, for K^- lab momenta of 1.8, 1.9, 2.0, 2.1 and 2.2 GeV/c. The parametrization of Eq. (25) is used, transformed to the lab system. For each momentum, the curve terminates at the maximum allowed lab angle $\theta^{\phi}_{L,\rm max}$.

Fig. 5: The double differential cross section $d^2\sigma/d\Omega_L\, dp_{K^+}$ for the (K^-, K^+) reaction at 1.65 GeV/c on various nuclear targets, as a function of K^+ lab momentum. The open squares represent the data of Iijima et al. [7], in momentum bins of 50 MeV/c. The dashed and dotted curves represent the contributions of the $K^-p \to K^+\Xi^-$ and $K^-p \to K^+\Xi^{*-}(1535)$ quasifree processes [7]. The solid curves represent our predicted K^+ momentum spectra, using Model 2 for the $K^-p \to \phi\Lambda$ cross section, and including the contribution of f_0 and a_0 production. The data and the theoretical predictions are averaged over the angular interval $1.7 \leq \theta_L \leq 13.6°$.

Fig. 6: The (K^-, K^+) double differential cross section on a ^{107}Ag target at 1.65 GeV/c. The open squares correspond to the data of Iijima et al. [7], after subtraction of their predicted Ξ^- and $\Xi^{*-}(1535)$ quasifree components. The upper three theoretical curves represent the predictions for Model 1

(dashed), Model 2 (solid) and Model 3 (dotted) of the $K^- p \rightarrow \phi\Lambda$ cross section, with the contribution of f_0 and a_0 production included as described in the text. The lower solid curve displays the ϕ contribution alone for Model 2.

Fig. 7: Predicted dependence of the double differential cross section $d^2\sigma/d\Omega_L\, dp_{K^+}$ for the (K^-, K^+) reaction on ^{12}C and ^{208}Pb on the incident K^- momentum. Curves for $p_{K^-} = 1.4$, 1.6 and 1.8 GeV/c are shown. Model 2 was used, and the cross sections were averaged over the angular interval $1.7 \leq \theta_L \leq 13.6°$. The curves represent the summed contributions of ϕ, f_0 and a_0 production.

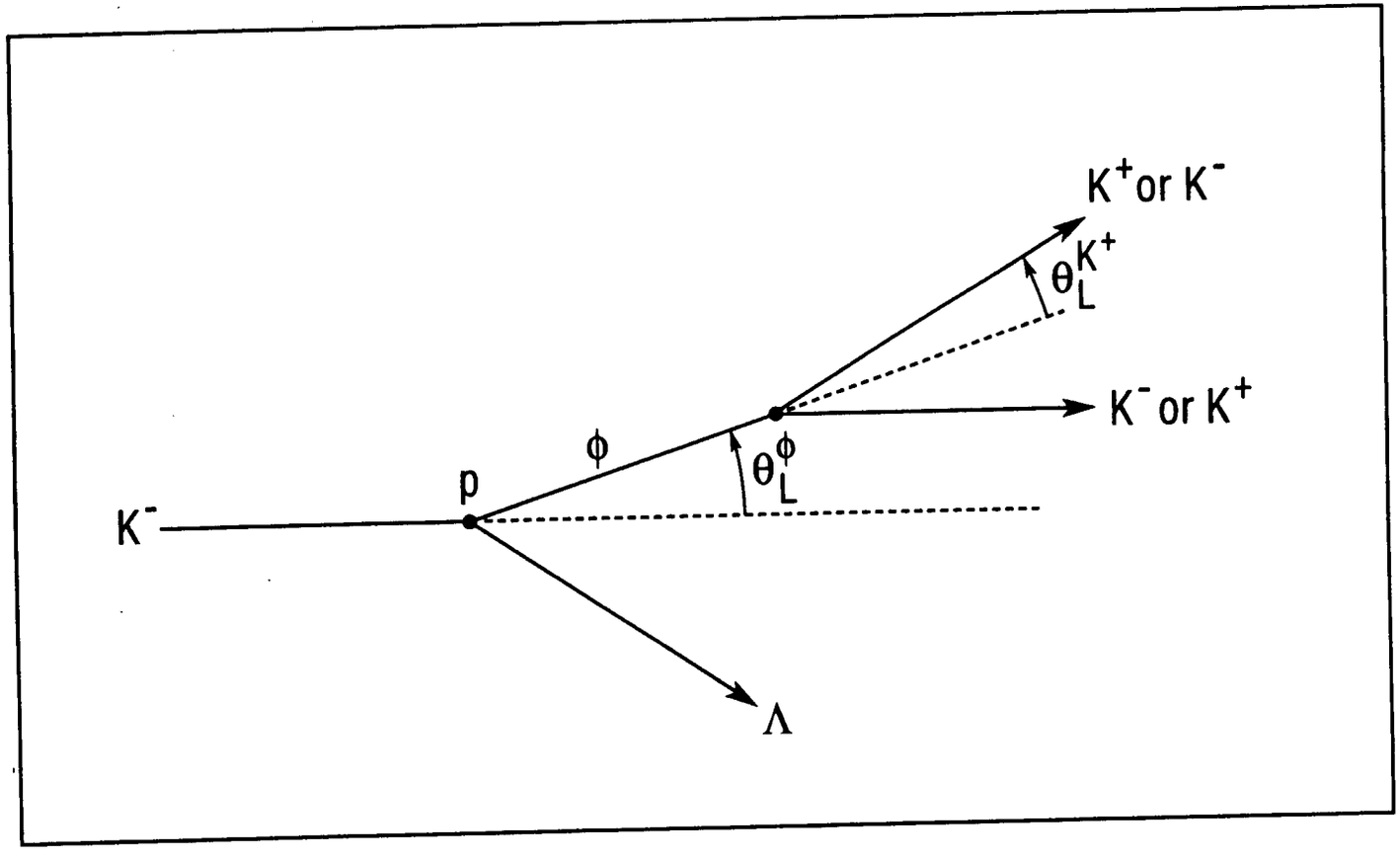

Fig. 1

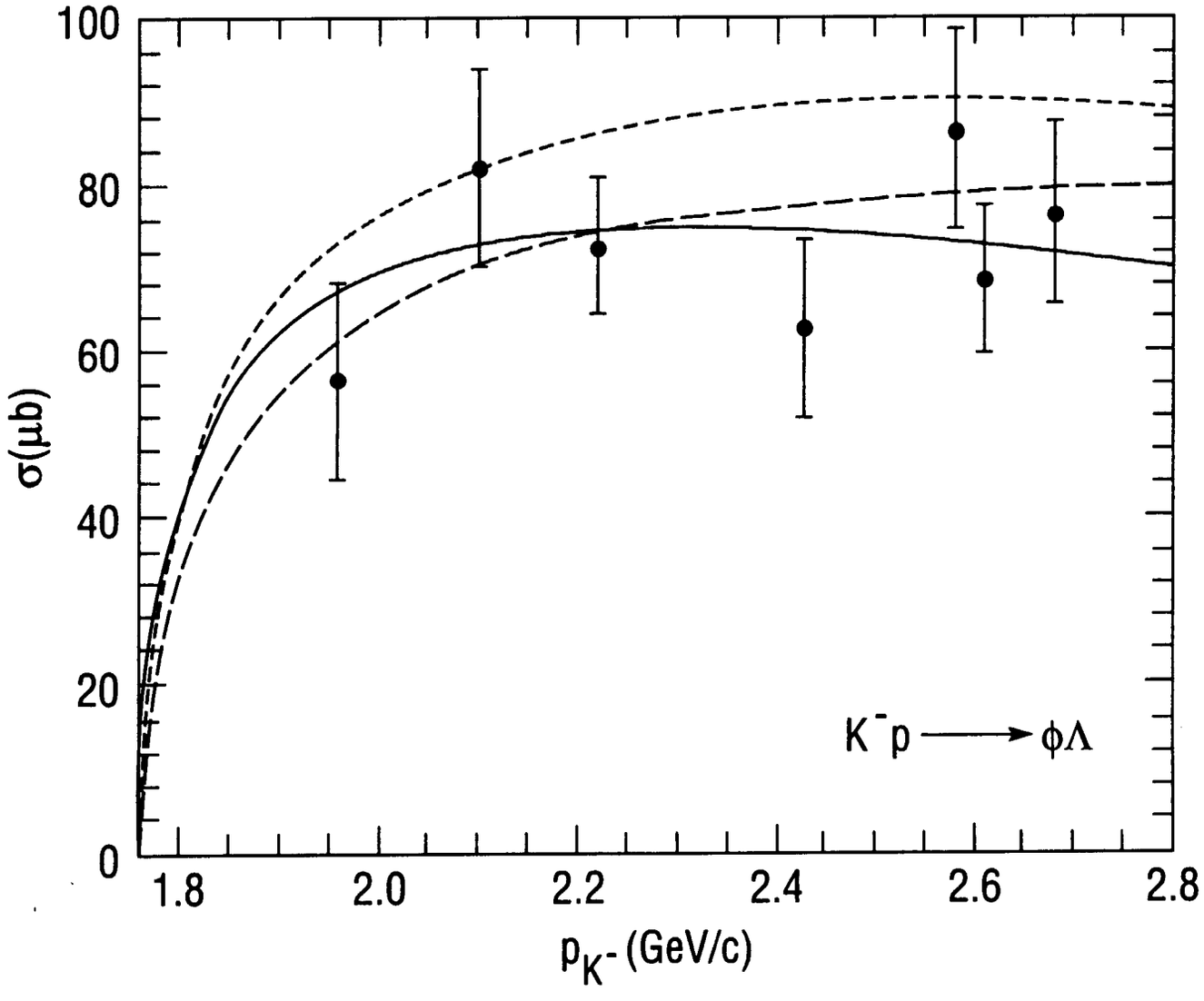
100
80
60
40
20
0
σ(μb)
1.8
2.0
2.2
2.4
2.6
2.8
p_{K^-} (GeV/c)
$K^- p \longrightarrow \phi\Lambda$

Fig. 2

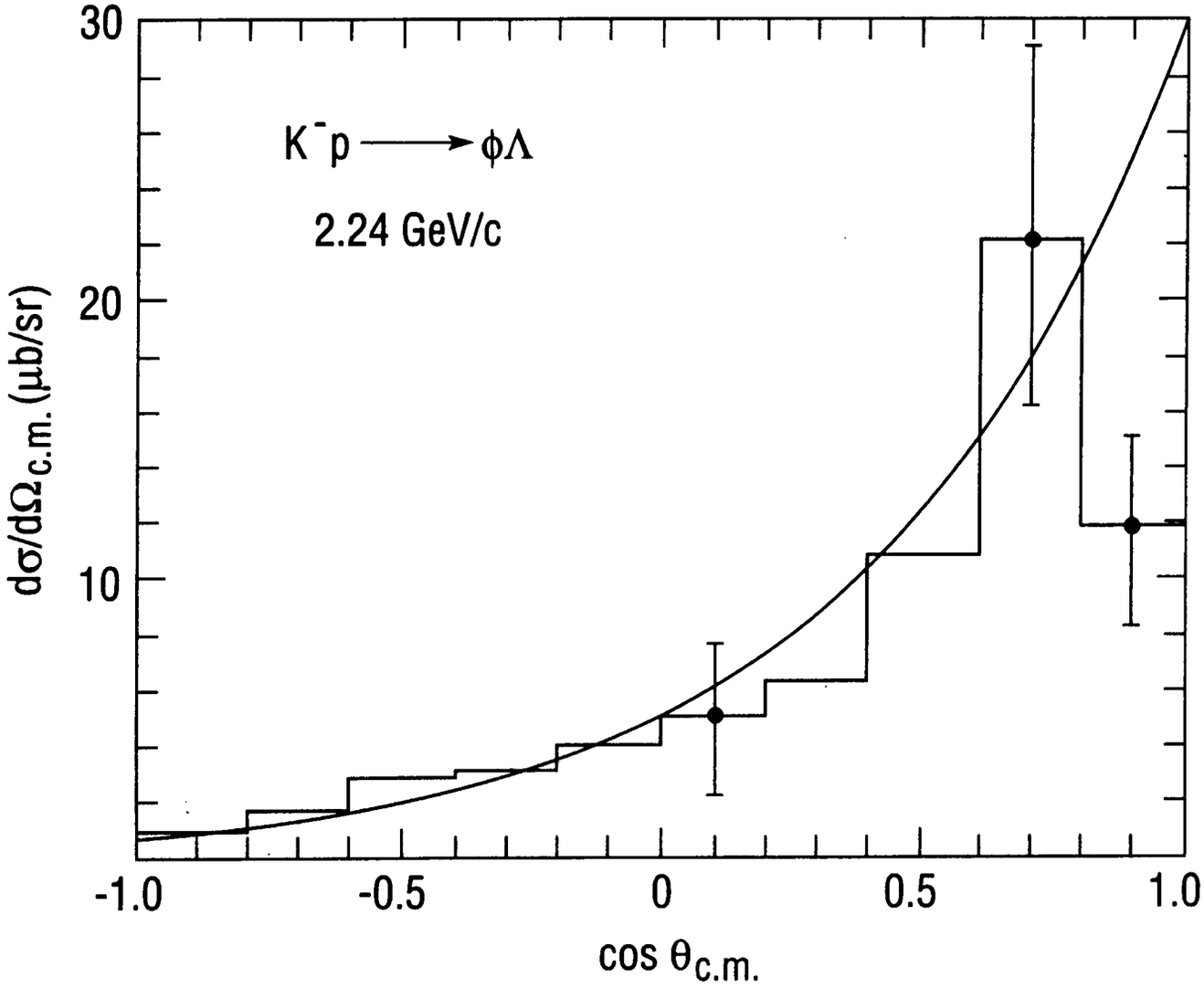
30
20
10
$K^- p \longrightarrow \phi\Lambda$
2.24 GeV/c
$d\sigma/d\Omega_{c.m.}$ (μb/sr)
-1.0
-0.5
0
0.5
1.0
$\cos\theta_{c.m.}$

Fig. 3

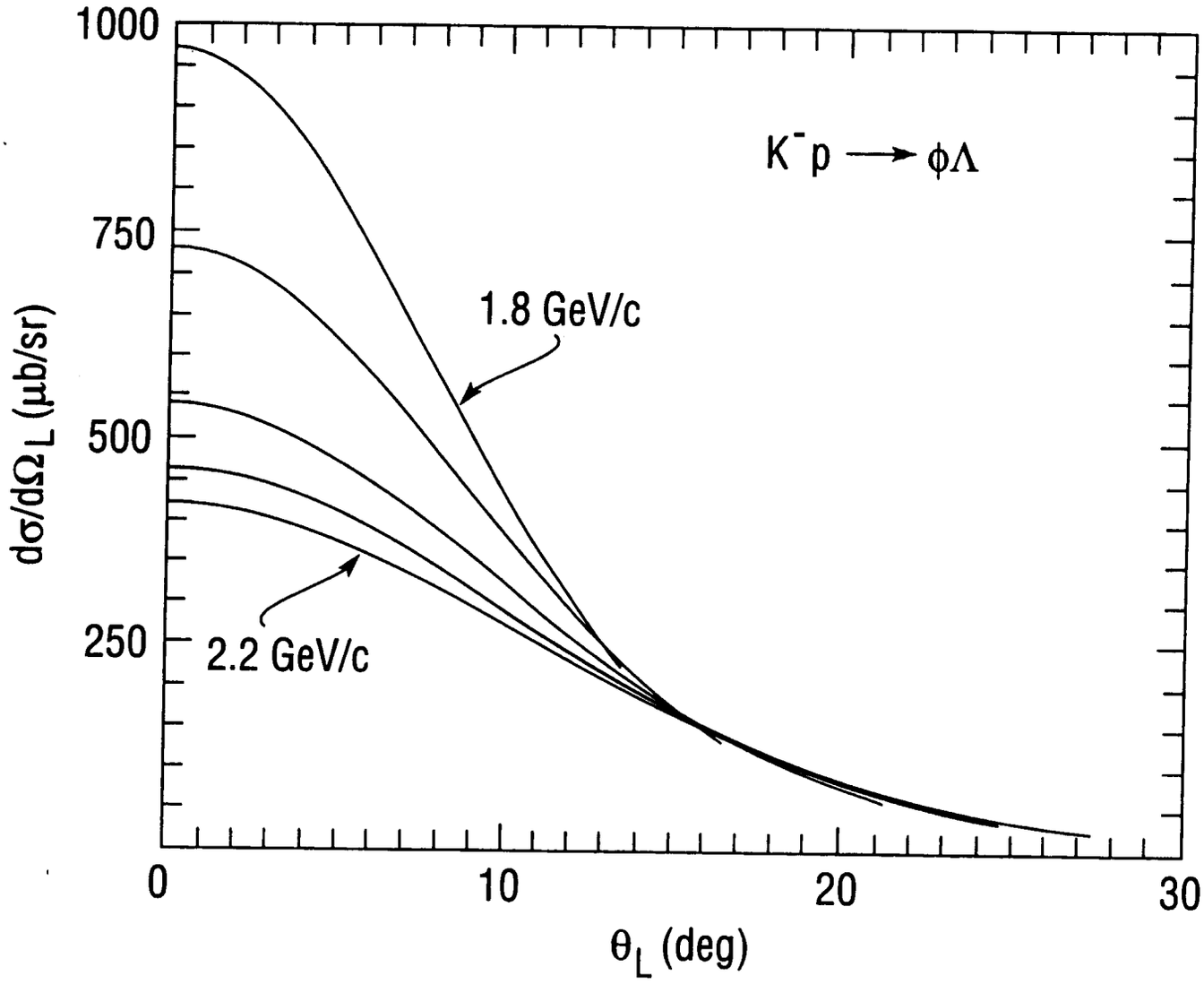
1000
750
500
250
0
10
20
30
$K^- p \rightarrow \phi\Lambda$
1.8 GeV/c
2.2 GeV/c
$d\sigma/d\Omega_L$ (μb/sr)
θ_L (deg)

Fig. 4

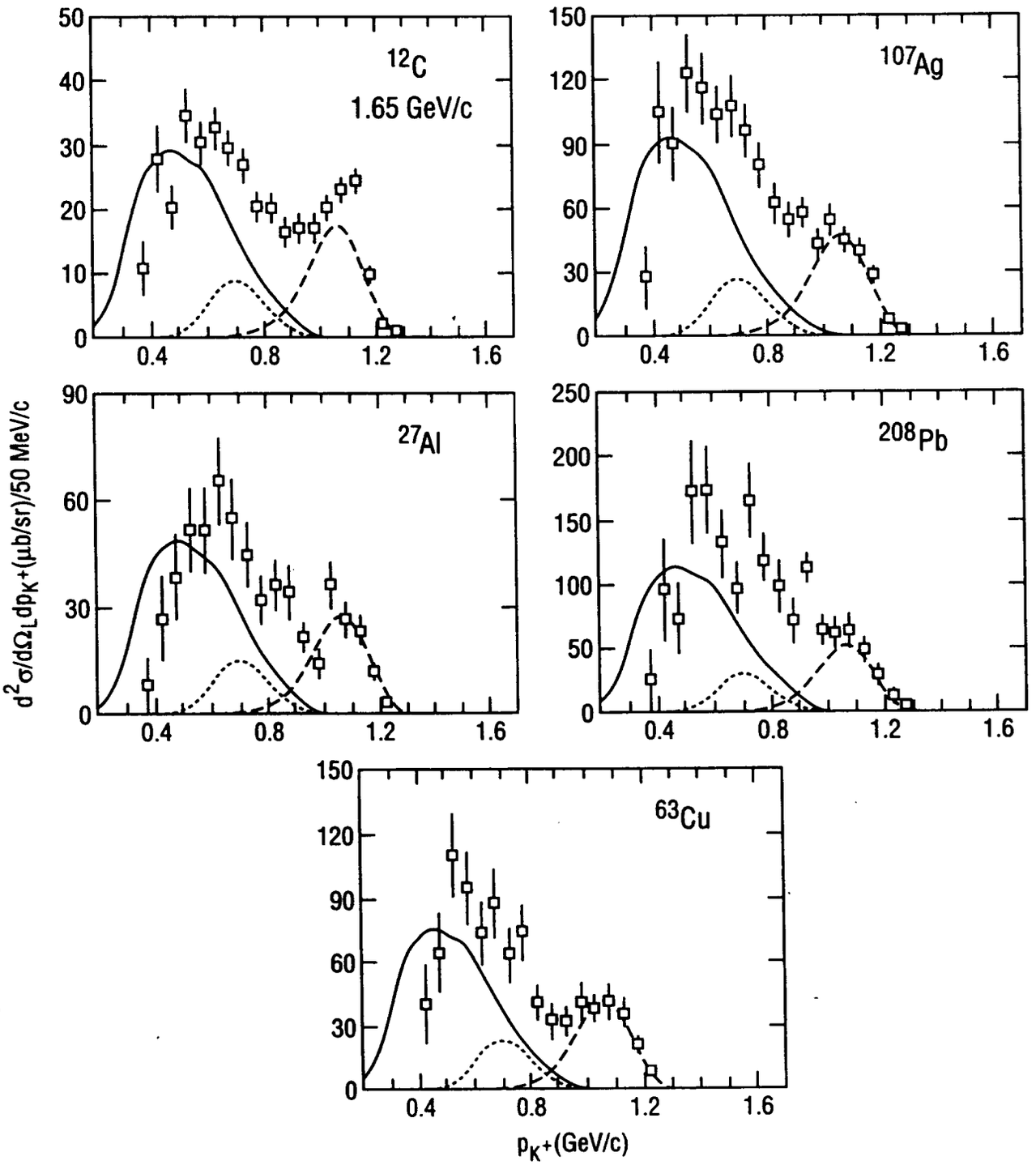
^{12}C
1.65 GeV/c
^{107}Ag
^{27}Al
^{208}Pb
^{63}Cu
$d^2\sigma/d\Omega_L dp_{K^+}$(μb/sr)/50 MeV/c
p_{K^+}(GeV/c)

Fig. 5

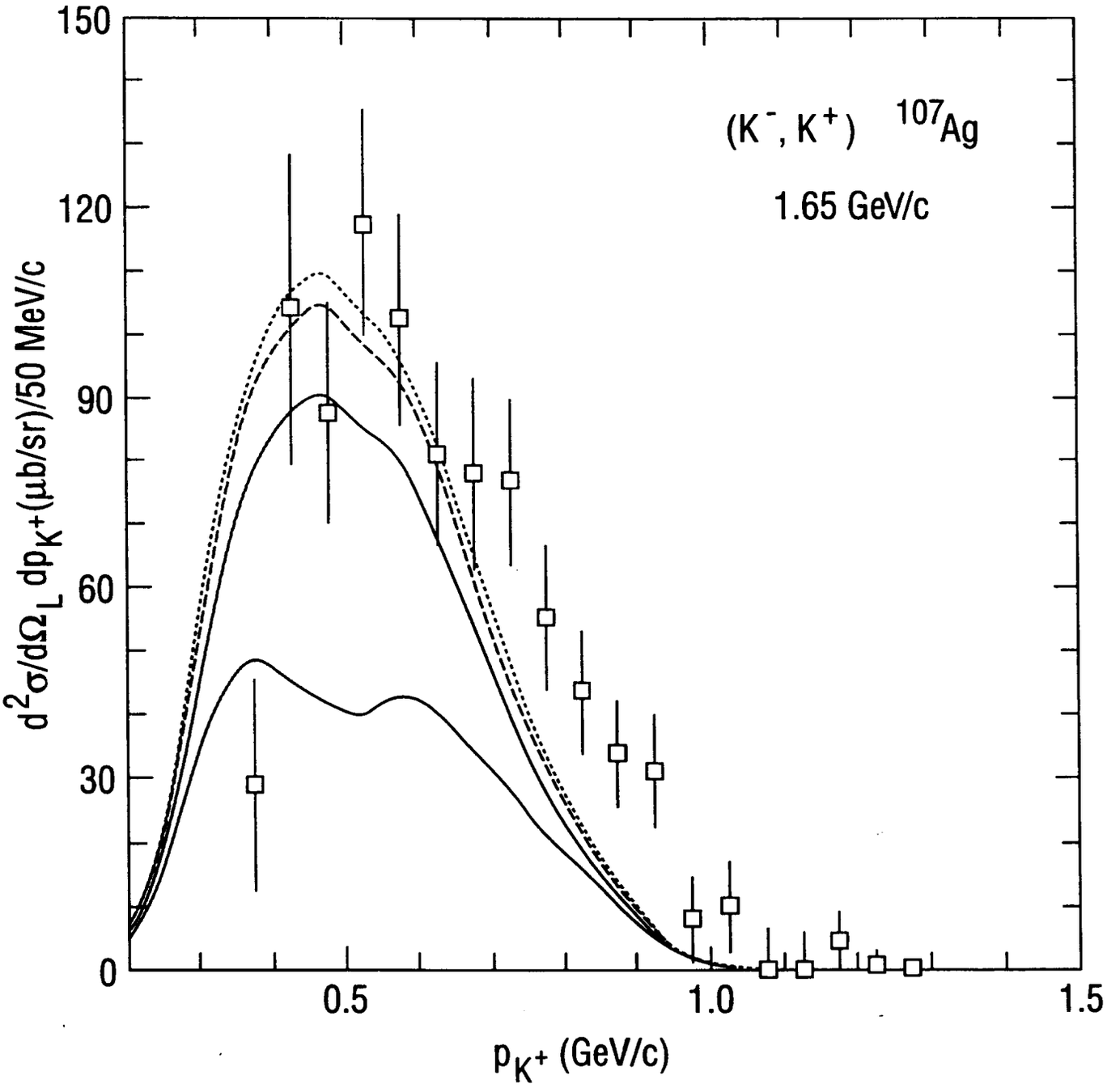
150
120
90
60
30
0
0.5
1.0
1.5
(K^-, K^+) ^{107}Ag
1.65 GeV/c
$d^2\sigma/d\Omega_L\, dp_{K^+}$(μb/sr)/50 MeV/c
p_{K^+} (GeV/c)

Fig. 6

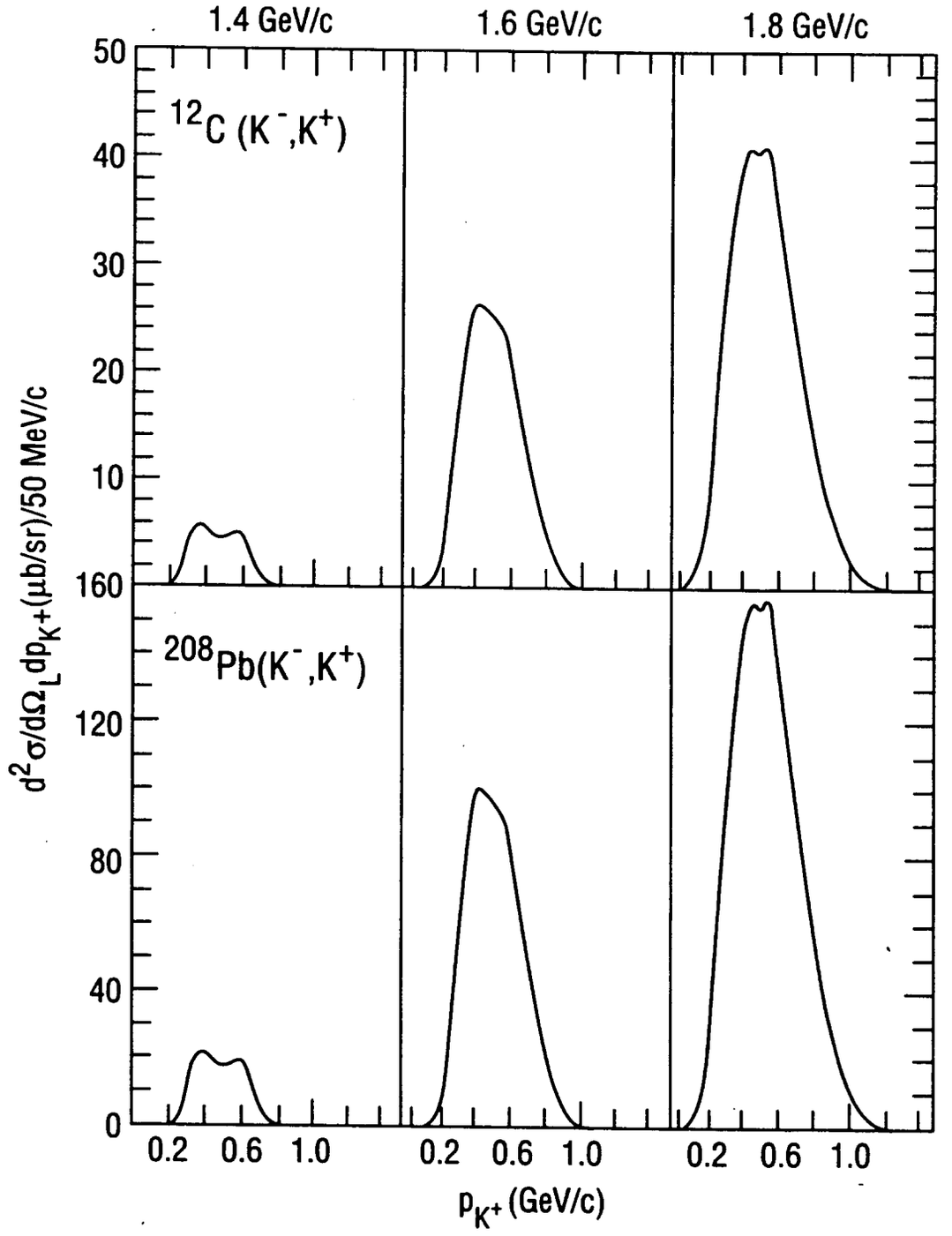
1.4 GeV/c
1.6 GeV/c
1.8 GeV/c
^{12}C (K^-,K^+)
^{208}Pb(K^-,K^+)
$d^2\sigma/d\Omega_L dp_{K^+}$(μb/sr)/50 MeV/c
p_{K^+} (GeV/c)
50
40
30
20
10
160
120
80
40
0
0.2
0.6
1.0

Fig. 7